General Technique of Quasielastic Spectrum Study: Application to Be^9

HOAN NGUYEN-NGOC AND JEAN P. PEREZ-Y-JORBA
Ecole Normale Supérieure Laboratoire de l'Accélérateur Linéaire, Orsay, Seine et Oise, France
(Received 11 March 1964)

We have established a formula which allows the extraction of the nuclear cross sections from experimental quasielastic spectra. Tests have been carried out to prove the consistency of our techniques. In particular, we prove that a hitherto unmeasured cross section can be calculated from a limited number of experimental data. These techniques have been applied to Be^9. Interpretations of the extracted cross sections have been estimated on three models.

INTRODUCTION

In a considerable number of studies of nuclear structure, Coulomb excitation through electron scattering has given results in the last years.[1,2] The electromagnetic nature of the interaction allows considerable calculation of electron scattering on nuclei. However, if a large variety of nuclei has been studied in this way, the domain of excitation energy remains below 10 MeV and a particular effort seems to be concentrated on elastic scattering and inelastic discrete levels studies.

It has been demonstrated that elastic scattering of high-energy electrons is extremely useful to determine the spatial structure of the nuclear ground-state charge density and its associated mean-square radius. On the other hand, inelastic induced reactions to discrete levels have been extensively studied in Born approximation. The multipolarity and decay rate of the corresponding de-excitation γ rays determined by such analysis, agree surprisingly well with results given by other methods.[3]

In spite of the possibility of the forthcoming interesting information, on the mean nucleon binding energy, the nucleon momentum distribution in the nucleus, or on the correlations between nucleons, the experimental inelastic continuum has not so far been explored systematically. Some attempts at explaining the continuum inelastic scattering cross section have already been made, either by using the single-particle excitation model,[4,5] or by impulse approximation to evaluate nucleon ejection probability.[6,7]

In the first part of this article, a general method has been evolved, which is suitable for light nuclei in the first Born approximation, of extraction of all the inelastic cross sections (electrodisintegration+continuum) for any given scattering angle of the electrons and for a large range of excitation energy of the nucleus and of incident energy, all from a limited number of experimental data. This method is a generalization of the techniques used up till now for the inelastic discrete levels. This problem is dominated mainly by the radiative corrections, of which the formulation is given on general lines. Checks of the validity of the method are given.

In the second part the above techniques are applied to the special case of Be^9, and the corresponding cross sections for its continuum are extracted. The results obtained are then compared with three theoretical models. Finally, an effort has been made to detect the giant resonance.

APPARATUS AND EXPERIMENTAL METHOD

The measurements have been carried out by the 250-MeV section of the Orsay linear accelerator, using standard arrangements described in Refs. 8 and 9. The incident electron beam is analyzed by two steering magnets associated with a collimator and a tungsten slit, giving an energy resolution as good as 0.2%.

The current is measured by the use of a Faraday cup in association with a secondary emission monitor.

Metallic targets with thicknesses varying from 0.5 to 3 mm are placed in a vacuum target chamber connected with the accelerator vacuum. In every case the target is set perpendicular to the bisector of the scattering angle.

Scattered electrons are analyzed as far as their momenta are concerned, by a double focusing magnetic

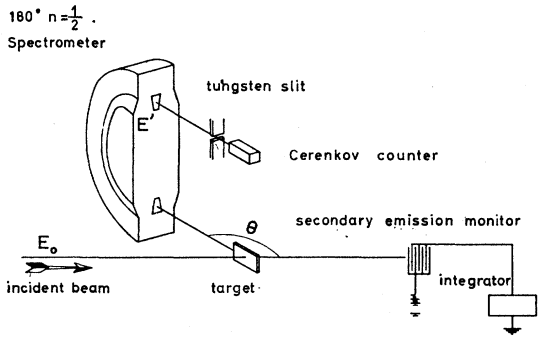

FIG. 1. Experimental arrangement.

[1] R. Hofstadter, Ann. Rev. Nucl. Sci. **7**, 231 (1957).
[2] W. C. Barber, Ann. Rev. Nucl. Sci. **12**, 1 (1962).
[3] H. W. Kendall and I. Talmi, Phys. Rev. **128**, 792 (1962); H. Crannell, R. Helm, H. Kendall, J. Oeser, and M. Yearien, *ibid.* **123**, 923 (1961).
[4] G. R. Bishop, Internal Report, Linear Accelerator Laboratory 1038, October 1962 (unpublished).
[5] W. Czyz, Phys. Rev. **131**, 2141 (1963).
[6] A. Goldberg, Phys. Rev. **112**, 618 (1958). A. G. Sitenko and V. N. Gur'ev, Zh. Eksperim. i Teor. Fiz. **39**, 1760 (1960) [English transl.: Soviet Phys.—JETP **12**, 1228 (1961)]. P. Bounin, J. Phys. Radium **24**, 974 (1963).
[7] J. Potter, thesis, Université de Paris, 1963 (unpublished).
[8] D. B. Isabelle, thesis, Université de Paris, 1961 (unpublished). D. B. Isabelle and G. R. Bishop, Nucl. Phys. **45**, 209 (1963).
[9] F. Lacoste, thesis, Université de Paris, 1962 (unpublished). F. Lacoste and G. R. Bishop, Nucl. Phys. **26**, 511 (1961).

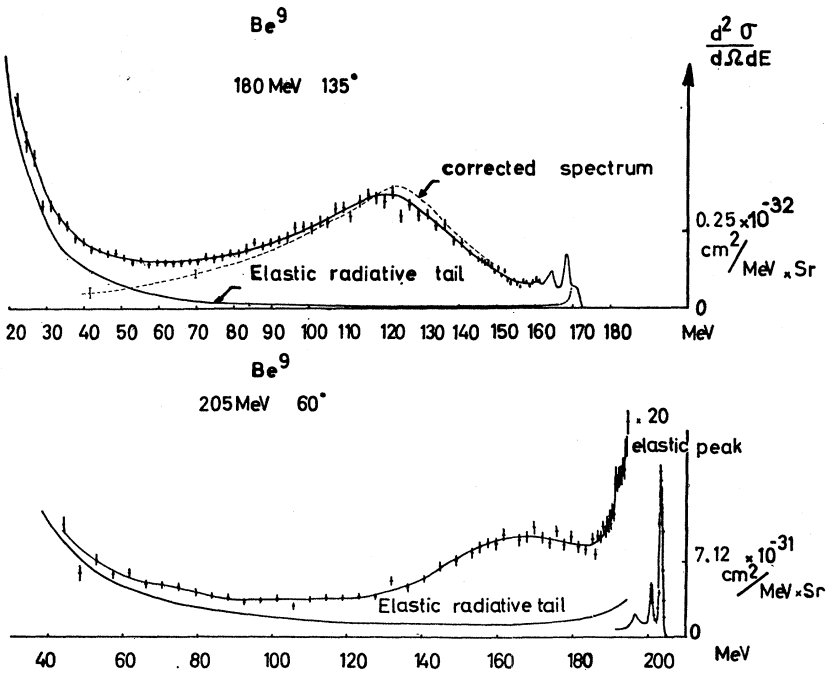

FIG. 2. Experimental spectra of electron scattering on Be^9. The elastic radiative tails are shown as well as the extracted spectrum (see part II).

spectrometer, and counted by a Lucite Cherenkov counter associated with a 56 AVP photomultiplier. A tungsten slit placed in front of the Lucite counter determines the momentum resolution which varies from 0.2 to 0.5% in most of our measurements (Fig. 1).

The Cherenkov counter used in connection with a high discriminator level and good shielding of the counter eliminates background. This is confirmed by the absence of counts when no target is present in the beam.

PART I—DATA PROCESSING

From the experimental point of view, the measured data constitute a number of electron scattering spectra, each spectrum corresponding to a given incident energy and scattering angle. Thus, the counting rate of scattered electrons, as a function of their energies, is measured (Fig. 2).

At the maximum energy of the scattered electrons, one finds the elastic peak. At lower energies one has successively low-lying discrete levels, if any, then a continuous excitation enhancement, and then the cross section decreases. Here we are interested in this continuum region.

In fact, this measured spectrum does not provide the nuclear interaction cross section since the electrons can emit and reabsorb virtual photons and also lose energy by radiation while interacting with the nucleus field, by ionization or excitation of the atomic electrons. These effects of energy losses give rise to an extension of the elastic or inelastic peaks towards the low-energy side and distort the spectrum. In considering the cross sections at a given scattered energy E_f, one must take into account the fact that this cross section has received the contributions of those electrons scattered at energy $E_f' > E_f$, which have lost precisely an amount of energy $E_f' - E_f$ in the described processes. On the other hand, these same processes reduce the energy of the electrons scattered at E_f and hence the considered cross section is lowered by this fractional loss.

The latter kind of process we have called "correction of type A" and the former kind "correction of type B."

A. "A Correction Terms"

We now enumerate the corrections applied to the measured cross sections. Let us consider first the "A correction term" in the case of an elastic peak. They are produced by a twofold process.

(1) The correction due to the fact that the electron radiates during the scattering and that it is not detected if the radiation energy emitted is superior to an energy ΔE fixed by the experimental conditions.

(2) The corrections due to the electrons scattered at the right energy (that of the elastic peak for example) but which lose an additional amount of energy, which is larger than the experimental resolution by bremsstrah-

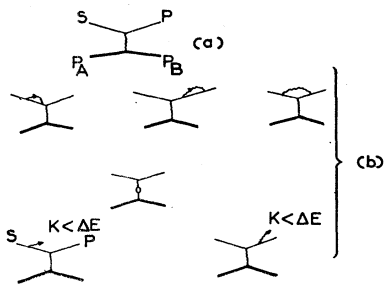

FIG. 3. (a) Diagram of electron scattering on the nucleus. (b) Diagrams of lowest order radiative correction.

lung on other nuclei, or by collisions with atomic electrons.

(1) Radiative correction: Experimentally, one always measures the sum of the diagrams (Fig. 3), the higher order diagrams being ignored.

The three diagrams in Fig. 3(b) represent the reactive effect of the electron with its field, and the fourth represents the vacuum polarization. They were first calculated by Schwinger[10] in the particular case of potential scattering. The last two diagrams are provided with a view to abolishing the infrared divergence, where ΔE is considered as the experimental resolution. In other words, the uncertainty ΔE in the scattered energy signifies that one only detects the electrons which have lost, by real photon emission, an amount of energy inferior to ΔE. The renormalized diagram is simply related to the second ones by

$$\frac{d\sigma}{d\Omega_{\text{observed}}}(E,\Delta E,\theta)=\frac{d\sigma_0}{d\Omega}(E,\theta)(1-\delta_s). \tag{1}$$

Here we call $(d\sigma/d\Omega_{\text{obs}})(E,\Delta E,\theta)$ the cross section measured in an energy band ΔE, and $(d\sigma_0/d\Omega)(E,\theta)$ the cross section corresponding to the nonradiative diagram.

The expression for δ_s is given by

$$\delta_s=\frac{4\alpha}{\pi}\left\{\left(\ln\frac{2E\sin\theta/2}{mc^2}-\frac{1}{2}\right)\left(\ln\frac{E}{\Delta E}-\frac{13}{12}\right)+\frac{17}{72}+\phi(\theta)\right\}, \tag{2}$$

where $\phi(\theta)$ is given in integral form and has been tabulated[9] as function of the scattering angle.

The conjecture made by Schwinger to replace $1-\delta_s$ by $e^{-\delta_s}$ to include higher order diagrams has been confirmed.[11]

A more complete expression for δ_s has also been given[12] allowing a recoil for the proton target.

(2) Since the electrons are detected in a small energy band ΔE we lose a proportion of them by continuous diminution of their energy through the limited thickness of the target. Basically, one may write

$$\frac{d\sigma}{d\Omega_{\text{obs}}}(E,\Delta E,\theta)=\int_0^t dx\int_0^{\Delta E}d\Delta\int_0^{\Delta}d\Delta'\times P(E,\Delta',x)\frac{d\sigma_0}{d\Omega}(E-\Delta',\theta)P(E-\Delta',\Delta-\Delta',t-x), \tag{3}$$

where $P(E,\Delta,x)$ accounts for the probability of an electron, of incident energy E, losing an amount of energy Δ in traversing a target thickness x. Simplifications are introduced by asuming that the target thickness t is thin enough to allow the factorization of the cross section. On the other hand, the probability of the twofold process can be estimated quite well by the product of the two probabilities. Then,

$$\frac{d\sigma}{d\Omega_{\text{obs}}}(E,\Delta E,\theta)=\frac{d\sigma_0}{d\Omega}(E,\theta)[1-\delta_i]e^{-\delta_B}, \tag{4}$$

where

$$e^{-\delta_B}=\int_0^{\Delta E}P_{\text{radiation}}(E,\Delta,t)d\Delta$$

and

$$\delta_i=\int_{\Delta_E}^{E}P_{\text{ionization}}(E,\Delta,t)d\Delta. \tag{5}$$

Here we call $P_{\text{radiation}}$ and $P_{\text{ionization}}$ the probabilities for energy loss by radiation and ionization, respectively.

The probability $P_{\text{radiation}}\,d\Delta$ that an electron of initial energy E loses an energy between Δ and $\Delta+d\Delta$ after traversing a thickness t is given by[13]

$$P_{\text{radiation}}(E,\Delta,t)d\Delta=\frac{d\Delta}{E}\frac{1}{\Gamma(t/X_0\ln 2)}\left[\ln\frac{E}{E-\Delta}\right]^{\frac{t}{X_0\ln 2}} \tag{6}$$

where X_0 is the radiation length.

The gamma function is such that $\Gamma(x)\cong 1/x$ for $x\ll 1$. Hence, from (5) and (6) one finds $e^{-\delta_B}=(\Delta E/E)^{t/X_0\ln 2}$. The δ_i term refers to corrections related to the ionization process in which the electrons transfer small quantities of energy through a large number of collisions with atomic electrons. Landau's calculation[14] of the distribution probability of ionization loss can be written simply

$$\delta_i=\int_{\Delta E}^{E}P(E,\Delta,t)d\Delta=\frac{1}{\omega}, \tag{7}$$

where $\omega+\ln\omega=\lambda+0.37$.

These relations are valid for $\lambda=\Delta E/\xi>10$, where the characteristic energy ξ is defined by

$$\xi=t\times\frac{2\pi Ne^4\rho}{mv^2}\times\frac{\sum Z}{\sum A}, \tag{8}$$

where N Avogadro number, ρ cubic density of the target of thickness t, and v electron velocity.

Grouping all these corrections, we obtain the cross section for the measured value in an energy band ΔE

$$\frac{d\sigma}{d\Omega_{\text{obs}}}(E,\Delta E,\theta)=(1-\delta)\frac{d\sigma_0}{d\Omega}(E,\theta), \tag{9}$$

where we defined by $(1-\delta)=(1-\delta_i)e^{-(\delta_s+\delta_B)}$.

[10] J. Schwinger, Phys. Rev. **75**, 898 (1949).
[11] D. H. Yennie and H. Suura, Phys. Rev. **105**, 1378 (1957).
[12] Y. S. Tsai, Phys. Rev. **122**, 1898 (1961). N. Meister and D. H. Yennie, Phys. Rev. **130**, 1210 (1963).
[13] B. Rossi, *High Energy Particles* (Prentice Hall, Inc., Englewood Cliffs, New Jersey, 1952).
[14] L. Landau, J. Phys. (USSR) **8**, 201 (1944).

The expression (9) constitutes the "A correction term."

B. "B Correction Terms"

The main process which can provoke energy losses are, as we have seen, bremsstrahlung and ionization. Bremsstrahlung can occur during the collision as well as in the field of other nuclei. The cross section for scattering with radiation is proportional to the thickness t of the target, while radiation on other nuclei and ionization processes are proportional to the square of the thickness or to higher orders of t. Since our target thicknesses are smaller than 2% of the radiation length, we shall consider t and t^2 processes only.

1. Process Proportional to the Target Thickness

The bremsstrahlung cross section due to the interaction of relativistic electrons with an external static potential was first calculated by Bethe and Heitler[15] who gave a differential cross section in terms of the final electron and emitted photon variables. In the case where one detects only the electron, integration over the photon direction is necessary. This has been done by Racah,[16] and again by McCormick *et al.*[17] who found some misprints in the first article for the low-energy case. These calculations did not take into account the finite extension of the nucleus. In the meantime, Schiff[18] supplied a simple method of performing an approximate integration. Moreover, the Schiff formula easily lends itself to the inclusion of the form factors of the nucleus, in order to take into account its finite size. This last formulation has generally been used by experimentalists[8,19] to analyze their data.

The electron-proton bremsstrahlung cross section has now been studied more minutely.[20–22] In the case of an excited nucleus, Perez-y-Jorba[23] obtained a correction to the Bethe and Heitler formula integrated with the same approximation as indicated by Schiff. Recently, many people, quite independently, have taken a new interest in this problem. Bjorken,[24] in solving the general problem of multiple radiation in a target, has also calculated the radiation cross section in the peaking approximation. Maximon *et al.*[25] improve the peaking approximation given by Schiff, in calculating the neglected terms, but still using the static potential; the specific case of O^{16} has been examined by means of an electronic computer. Ginsberg *et al.*[26] calculate the radiation cross section, which is due to the static magnetic moment distribution as well as to the charge distribution, in the static approximation, and give numerical computation for specific cases. The Meister *et al.*[27] approach extends the Schiff peaking approximation to include the case where the external interaction field is no longer assumed to be a static potential, as in the Bethe-Heitler formula, and they consider in particular the case of electrodisintegration. Calculations along the same line have been made by other authors.[22,24]

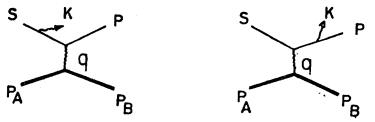

FIG. 4. Bremsstrahlung diagrams.

The complete differential radiation cross section in the first Born approximation, valid in the reference frame where the particle is at rest, has been obtained by Tsai.[28]

After this brief review, we now give the main line of our calculation, in which we allow for the fact that the nucleus can be left in an excited state, and that the incident nucleus may have a non-null initial momentum.

Let us consider the two following diagrams (Fig. 4):

The scattering amplitude is given by[29]

$$S^{(3)}=\frac{1}{(2\pi)^{7/2}}\left(\frac{m^2}{s_0p_0}\frac{N_AN_B}{p_{A0}p_{B0}2k_0}\right)^{1/2}T_{fi}\times\delta_4(s+p_A-p_B-p-k), \quad (10)$$

where $N_i=M_i$ for a fermion and $N_i=\frac{1}{2}$ for a boson. T_{fi} can be written as

$$T_{fi}=Z\frac{e^3}{q^2}\langle p|j_\mu|s\rangle\langle B|J_\mu|A,$$

or

$$\sum|T_{fi}|^2=Z^2e^6\frac{1}{q^4}S_{\mu\nu}T_{\mu\nu}, \quad (11)$$

with

$$S_{\mu\nu}=\tfrac{1}{2}\sum_{\text{spins, polarization}}\langle p|j_\mu|s\rangle\langle p|j_\nu|s\rangle^*. \quad (12)$$

Here, j_μ represents the electron current and is given by

$$j_\mu=\frac{\not{p}\not{k}\gamma_\mu}{2k\cdot p}+\frac{\gamma_\mu\not{k}\not{p}}{2k\cdot s}+\left(\frac{p\cdot e}{k\cdot p}-\frac{s\cdot e}{k\cdot s}\right)\gamma_\mu,$$

[15] W. Heitler, *The Quantum Theory of Radiation* (Oxford University Press, London, 1957).
[16] G. Racah, Nuovo Cimento **11**, 476 (1934).
[17] P. T. McCormick, D. G. Kieffer, and G. Parzen, Phys. Rev. **103**, 29 (1956).
[18] L. I. Schiff, Phys. Rev. **87**, 750 (1952).
[19] W. K. H. Panofsky and E. A. Allton, Phys. Rev. **110**, 1155 (1955); J. I. Friedman, *ibid.* **116**, 1257 (1959).
[20] S. D. Drell, Phys. Rev. **87**, 753 (1952).
[21] R. A. Berg and C. N. Lindner, Phys. Rev. **112**, 2072 (1958).
[22] L. N. Hand, Ph.D. thesis, Stanford University, 1961 (unpublished).
[23] J. Perez-y-Jorba, J. Phys. Radium **22**, 733 (1961).
[24] J. D. Bjorken, Ann. Phys. (N. Y.) **24**, 201 (1963).
[25] L. C. Maximon and D. B. Isabelle, Phys. Rev. **133**, B1344 (1964).
[26] E. S. Ginsberg and R. H. Pratt, Phys. Rev. **134**, B773 (1964). We are indebted to Dr. Ginsberg and Dr. Pratt for the numerical computation done with their program.
[27] N. Meister and T. Griffy, International Conference on Nucleon Structure Stanford University, 1963 (to be published); Phys. Rev. **133**, B1032 (1964).
[28] Y. S. Tsai, International Conference on Nucleon Structure Stanford University, 1963 (to be published).
[29] Jauch and Rohrlich, *Theory of Photons and Electrons* (Addison-Wesley Publishing Company, Reading, Massachusetts, 1955).

the polarization vector of the emitted photon being e_μ. The target line is contained in

$$T_{\mu\nu}=\frac{1}{2s_A+1}\sum_{s_A s_B}\langle B|J_\mu|A\rangle\langle B|J_\nu|A\rangle^*. \tag{13}$$

The calculation of $S_{\mu\nu}$ is straightforward by the trace method (29); one obtains

$$2m^2S_{\mu\nu}=-\frac{m^2}{(k\cdot s)^2}[S_{\mu\nu}{}^0-k_\mu p_\nu-k_\nu p_\mu]-\frac{m^2}{(k\cdot p)^2}[S_{\mu\nu}{}^0+k_\mu s_\nu+k_\nu s_\mu]-2g_{\mu\nu}$$
$$+\frac{1}{k\cdot p}[2p_\mu p_\nu+k_\mu s_\nu+k_\nu s_\mu+S_{\mu\nu}{}^0+(s\cdot p-m^2)g_{\mu\nu}]-\frac{1}{k\cdot s}[2s_\mu s_\nu-k_\mu p_\nu-k_\nu p_\mu+S_{\mu\nu}{}^0+(s\cdot p-m^2)g_{\mu\nu}]$$
$$-\frac{1}{k\cdot pk\cdot s}[2m^2k_\mu k_\nu+s\cdot p(k_\mu p_\nu+k_\nu p_\mu-k_\mu s_\nu-k_\nu s_\mu-2S_{\mu\nu}{}^0)], \tag{14}$$

where we have put $S_{\mu\nu}{}^0=s_\mu p_\nu+s_\nu p_\mu+\frac{1}{2}q^2g_{\mu\nu}$, with $q=s-p-k$.

The cross section can then be written as

$$\frac{d^2\sigma}{d\Omega dp}=\frac{\alpha^3}{(2\pi)^2}\frac{4m^2N_AN_B}{[(s\cdot p_A)^2-m^2M_A{}^2]^{1/2}}\times\int\frac{\mathbf{p}^2}{p_0}\cdot\frac{\mathbf{k}^2}{k\cdot p_B}\frac{1}{q^4}S_{\mu\nu}T_{\mu\nu}d\Omega_k \tag{15}$$

for a discrete inelastic level, and as

$$\frac{d^2\sigma}{d\Omega dp}=\frac{\alpha^3}{(2\pi)^2}\frac{4m^2N_AN_B}{[(s\cdot p_A)-m^2M_A{}^2]^{1/2}}\times\int\frac{\mathbf{p}^2}{p_0}\frac{k_0dk_0}{p_B{}^0}\frac{1}{q^4}S_{\mu\nu}T_{\mu\nu}{}^cd\Omega_k \tag{16}$$

for continuum states.

Here $T_{\mu\nu}{}^c$ is given by (13), but where the matrix element of the operator J_μ is taken between the initial discrete state and the final state corresponding to the continuum. It, then, has a different dimension from that of $T_{\mu\nu}$ of Eq. (15).

In the latter case one must bear in mind the connection between k_0 and Ω_k through the energy momentum conservation.

If the recoil target is not detected, $T_{\mu\nu}$ must be constructed from two of the three vectors q, p_A, and p_B since they are interdependent through the momentum conservation. By gauge invariance, it can be shown[30] that one form of $T_{\mu\nu}$ is

$$T_{\mu\nu}=F(q^2,q\cdot p_A)p_{A\mu}p_{A\nu}+G(q^2,q\cdot p_A)g_{\mu\nu}, \tag{17}$$

where F and G are two real functions of the scalar variables q^2 and $q\cdot p_A$. The other terms including q_μ or $q_\mu q_\nu$ give a null contribution in the contraction with $S_{\mu\nu}$.

In the case where the target is a nucleon, the tensor $T_{\mu\nu}$ of the nucleon current can be shown (for example, Ref. 7) to be

$$T_{\mu\nu}=\frac{1}{M^2}\left\{\left[F_1{}^2(q)-\frac{q^2}{4M^2}K^2F_2{}^2(q)\right]p_\mu{}^Ap_\nu{}^A-\frac{q^2}{4}[F_1(q)+KF_2(q)]^2g_{\mu\nu}\right\}, \tag{18}$$

where K is the anomalous magnetic moment, and F_1 and F_2 are the form factors introduced in the Rosenbluth formula.[1] If one defines the charge and magnetic form factors

$$F_{\rm ch}=F_1-(q^2/4M^2)KF_2,\qquad F_m=F_1+KF_2, \tag{19}$$

then the G form factor of Eq. (17) can be identified with a magnetic form factor, while the F term is a combination of charge and magnetic form factors. Contraction of $T_{\mu\nu}$ with $S_{\mu\nu}$ gives

$$S_{\mu\nu}T_{\mu\nu}=\frac{F}{2m^2}\left\{\frac{-m^2}{(k\cdot s)^2}\left[2(p\cdot p_A)(s-k)\cdot p_A+\frac{q^2}{2}p_A{}^2\right]-\frac{m^2}{(k\cdot p)^2}\left[2(s\cdot p_A)(p+k)\cdot p_A+\frac{q^2}{2}p_A{}^2\right]\right.$$
$$-2p_A{}^2+\frac{1}{k\cdot p}\left[2(p\cdot p_A)^2+2(s\cdot p_A)(p+k)\cdot p_A+\left(\frac{q^2}{2}-m^2+s\cdot p\right)p_A{}^2\right]$$
$$-\frac{1}{k\cdot s}\left[2(s\cdot p_A)^2+2(p\cdot p_A)(s-k)\cdot p_A+\left(\frac{q^2}{2}-m^2+s\cdot p\right)p_A{}^2\right]$$
$$\left.+\frac{2}{(k\cdot p)(k\cdot s)}\left[-m^2(k\cdot p_A)^2+s\cdot p\left(k\cdot p_As\cdot p_A-k\cdot p_Ap\cdot p_A+2p\cdot p_As\cdot p_A+\frac{q^2}{2}p_A{}^2\right)\right]\right\}$$
$$+\frac{G}{2m^2}\left\{-m^2(2m^2+q^2)\left[\frac{1}{(k\cdot s)^2}+\frac{1}{(k\cdot p)^2}\right]-4+\left(\frac{1}{k\cdot p}-\frac{1}{k\cdot s}\right)(q^2+6s\cdot p-2m^2)+\frac{4s\cdot p}{k\cdot pk\cdot s}(s\cdot p+q^2)\right\}. \tag{20}$$

[30] M. Gourdin, Nuovo Cimento **21**, 1094 (1961).

The cross sections are immediately obtained by putting the expression (20) in Eqs. (15) or (16).

This is the general form that can be obtained from the diagrams under consideration, F and G being two form factors, which, in principle, one can calculate if the current for the target line is known. We shall see later that we can deduce them from experimental measurements.

In the particular frame where the initial target is at rest, $p_A=(M_A,O)$ one finds the expression already given by Tsai.[28]

In this frame of reference, one may use as z axis the vector $\mathbf{u}=\mathbf{s}-\mathbf{p}$ by defining

$$u=s-p+p_A. \tag{21}$$

Hence, the square of four momentum transfer depends only on $\cos(\mathbf{u},\mathbf{k})$ since

$$q^2=(u-k-p_A)^2. \tag{22}$$

We have to integrate over $d\Omega_k=d\phi_k d\cos(\mathbf{k},\mathbf{u})$. As the nuclear form factors depend on q^2 and then on $\cos(\mathbf{k},\mathbf{u})$ and not on ϕ_k, the integration on ϕ_k is straightforward, since all the integrals are of the form

$$\int_0^{2\pi}\frac{d\phi}{a+b\cos\phi}=\frac{2\pi}{(a^2-b^2)^{1/2}}$$

and

$$\int_0^{2\pi}\frac{d\phi}{(a+b\cos\phi)^2}=\frac{2\pi a}{(a^2-b^2)^{3/2}}, \tag{23}$$

where $a^2>b^2$. The complete result is given in the Appendix.

This far, our formulation is free from approximation.

Using a different calculation, Maximon *et al.*[25] have already obtained the same result in the special case of potential scattering.

At this stage one is still left with an integration over $d\cos(\mathbf{k},\mathbf{u})$ which can be terminated only if one knows the explicit dependence of the form factors on q^2.

On the opposite case one can perform a numerical integration, but one can also use an approximate analytical integration. In the latter case, one performs immediately the direct integration over $d\Omega_k$ of $S_{\mu\nu}T_{\mu\nu}$ thanks to the peaking approximation suggested by Schiff.[18] It is, however, simple to perform the same approximation directly on $S_{\mu\nu}$.[24,27] We have done this approximation also, on our result.

The important contributions to $S_{\mu\nu}$ come from kinematic situations where the virtual electron is nearly on the mass shell, that is, when the photon is peaked in the electron direction (incident or scattered). In this peaking approximation, one replaces k_μ by $(k_0/s_0)s_\mu$ [or $(k_0/p_0)p_\mu$] for the case $\mathbf{k}\|\mathbf{s}$ (or $\mathbf{k}\|\mathbf{p}$) in the numerator terms everywhere there is a term of the form $k\cdot s$ (or $k\cdot p$) in the denominator. We obtain $S_{\mu\nu}$ as the sum of the two following terms:

$$\text{(a)}\quad \mathbf{k}\|\mathbf{s}\quad S_{\mu\nu}=\left[\left(1-\frac{k_0}{s_0}\right)\left(\frac{-m^2}{(k\cdot s)^2}+\frac{s_0-k_0}{k_0}\frac{1}{k\cdot s}\right)+\frac{s_0}{k_0}\frac{1}{k\cdot s}\right]\sum_{\mu\nu},$$

$$\text{(b)}\quad \mathbf{k}\|\mathbf{p}\quad S_{\mu\nu}=\left[\left(1+\frac{k_0}{p_0}\right)\left(\frac{-m^2}{(k\cdot p)^2}+\frac{p_0+k_0}{k_0}\frac{1}{k\cdot p}\right)+\frac{p_0}{k_0}\frac{1}{k\cdot p}\right]\sum_{\mu\nu}, \tag{24}$$

where

$$\sum_{\mu\nu}=\frac{1}{2m^2}[s_\mu p_\nu+s_\nu p_\mu+\tfrac{1}{2}(s-p)^2 g_{\mu\nu}] \tag{25}$$

corresponds to the electron tensor without radiation.

The integration over the photon direction can then be performed to give

$$\int S_{\mu\nu}d\Omega_k=\frac{4\pi}{k_0^2}\left[\left(1+\frac{E_2^2}{E_1^2}\right)\ln\frac{2E_1}{m}-\frac{E_2}{E_1}\right]\sum_{\mu\nu},$$

$$(m\ll E_1,E_2) \tag{26}$$

where

$$\text{(a)}\quad \mathbf{k}\|\mathbf{s}\quad E_1=s_0,\quad E_2=s_0-k_0,$$

$$\text{(b)}\quad \mathbf{k}\|\mathbf{p}\quad E_1=p_0,\quad E_2=p_0+k_0.$$

The advantage of the integration over $d\Omega_k$ on $S_{\mu\nu}$ appears in the factorization of $\sum_{\mu\nu}$ which will give after contraction with $T_{\mu\nu}$ the nonradiative cross section. This result has also been obtained by Bjorken[24] and Meister *et al.*[27] In fact, in our cases, the nonlogarithmic term is negligible compared with the first one.

The wide-angle bremsstrahlung can be written as

$$\frac{d^2\sigma}{d\Omega d_k}=\frac{\alpha}{k\pi}\left\{\left[1+\left(\frac{E_i-k}{E_i}\right)^2\right]\ln\frac{2E_i}{m}-\frac{E_i-k}{E_i}\right\}\frac{d\sigma_0}{d\Omega}(E_i-k,\theta)$$

$$+\frac{\alpha}{k\pi}\left\{\left[1+\left(\frac{E_f}{E_f+k}\right)^2\right]\ln\frac{2E_f}{m}-\frac{E_f}{E_f+k}\right\}\frac{d\sigma_0}{d\Omega}(E_i,\theta), \tag{27}$$

where we have slightly changed the notation $k=k_0$; $E_i=s_0$; $E_f=p_0$, $d\sigma_0/d\Omega$ stands for the nonradiative cross section.

For the particular case where $d\sigma_0/d\Omega$ represents only potential scattering we find the formula obtained by Perez y Jorba.[23]

For continuum states, one must replace $d\sigma_0/d\Omega$ by $d^2\sigma_0/d\Omega dp$ and integrate the right-hand side over dk from ΔE to the $k_{\max}$ determined by energy momentum conservation.

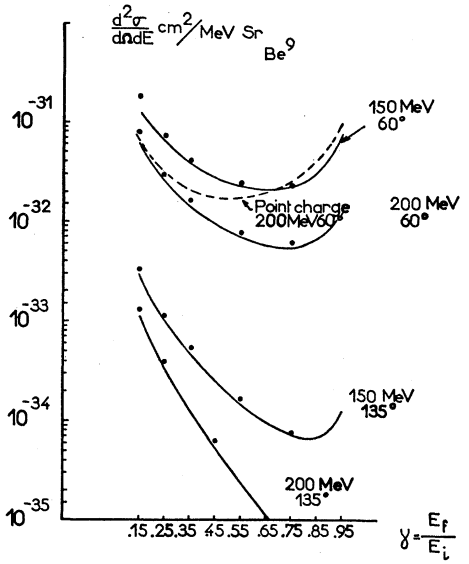

FIG. 5. Comparison of two Bethe-Heitler formula integrations for the elastic radiative tail. The plain curves have been calculated by numerical integration including the experimental elastic form factors. The points are calculated by using the peaking approximation.

When the Bethe-Heitler formula, including a form factor is used, one can compare a complete numerical integration of the above formula done by a computer, with the Schiff peaking approximation on the same formula. We have done that for the elastic radiative tail of Be^9 for different incident energies and scattering angles, and we were very kindly helped by Ginsberg and Pratt who did the numerical computation for us.[26] The difference between the two results is, in general, less than 3% of the nuclear cross sections in the region with which we are concerned (about 20% of the radiative tail itself) (Fig. 5).

The same result has been assumed to be valid when using the peaking approximation on the exact formula.

2. *Processes Proportional to the Square of the Thickness*

In traversing the target, there is a probability that the electron will undergo either a collision with an atomic electron, or a photon emission on a different nucleus from the one inducing the nuclear scattering. These processes may occur without any appreciable deviation of the electron from the initial direction, since the emitted photons or the recoil electrons are confined in a cone of half-angle of the order of mc^2/E, where E is the energy of the initial electron. Theoretically, these processes happen before and after the nuclear scattering, which takes place on the average, at the middle of the target. Since it is a second-order effect, we approximate by saying that the secondary collision arises only once, either before or after the nuclear scattering. Hence, schematically, we have a double process in which k is the energy loss, due to Möller collision or bremsstrahlung in the field of a second nucleus.

Assuming the two processes to be completely independent with small probability, one may write for the associated cross section[8]

$$\left(\frac{d^2\sigma}{d\Omega dk}\right)_{t^2}=\frac{t}{2}\{\phi_{\rm coll}(E_i,k)+\phi_{\rm rad}(E_i,k)\}\frac{d\sigma_0}{d\Omega}(E_i-k,E_f,\theta)+\frac{t}{2}\{\phi_{\rm coll}(E_f+k,k)+\phi_{\rm rad}(E_f+k,k)\}\frac{d\sigma_0}{d\Omega}(E_i,E_f+k,\theta) \quad (28)$$

where $\phi_{\rm coll}$ and $\phi_{\rm rad}$ are the probabilities[13] for an electron of energy E to lose an energy k in traversing unit target thickness.

$$\phi_{\rm rad}(E,k)=(1/kX_0)\varphi_{\rm rad}(E,k),$$

where $\varphi_{\rm rad}(E,k)$ is tabulated in Ref. 13.

$$\phi_{\rm coll}(E,k)=0.154\frac{Z}{A}\frac{1}{E^2}\left[\frac{1-x+x^2}{x(1-x)}\right]^2, \quad (29)$$

with $x=k/E$.

The cross section associated with the radiative tail is the sum of expressions (28) and (15) or (16); the expression (15) can be approximated by (27).

After the preceding analysis, we can write

$$\frac{d^2\sigma}{d\Omega dE_{f\rm obs}}(E_i,E_f,\theta)=\frac{d^2\sigma}{d\Omega dE_f}(E_i,E_f,\theta)[1-\delta]+\frac{d^2\sigma}{d\Omega dE_{f\rm rad.\ tail}}(E_i,E_f,\theta), \quad (30)$$

where

$$\frac{d^2\sigma}{d\Omega dE_{f\rm rad.\ tail}}=\int_\epsilon g(E_i-\epsilon,E_f)\frac{d\sigma_0}{d\Omega}(E_i;E_i-\epsilon;\theta)+g(E_i;E_f+\epsilon)\frac{d\sigma_0}{d\Omega}(E_f+\epsilon;E_f;\theta). \quad (31)$$

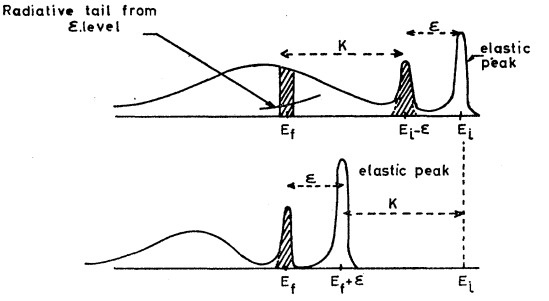

FIG. 6. The radiative tail contribution of an excited level ϵ, to the differential cross section at (E_f,θ), is in first approximation equal to the sum of two terms proportional to the cross section of this level at the respective incident energies of electrons E_i and $E_f+\epsilon$ and for the same θ; E_i being the incident energy associated to the spectrum under analysis.

TABLE I. Nuclear form factors defined as $\frac{d^2\sigma/d\Omega dE}{d\sigma/d\Omega_{\text{Mott}}}$ for each couple of incident energy and scattering angle and for different excitation energies.

ϵ MeV \ E_i MeV	$\theta=135°$					$\theta=60°$					$\theta=90°$			$\theta=75°$		105°
	177.3	148.5	121.4	99.0	73.1	230.6	181.0	152.0	99.5	70.0	230.7	176.7	100.0	176.4	146.0	176.4
4	0.24	1.19	2.11	5.78	3.12	2.53	2.49	3.00	4.20	0.85	0.33	1.13	3.32	1.77	3.41	0.83
8	0.86	1.61	2.57	5.36	3.22	2.95	2.40	2.63	3.40	0.82	0.66	1.66	3.28	2.06	3.48	1.35
12	1.36	1.92	2.47	3.62	2.61	2.73	2.25	1.98	1.90	0.59	0.81	2.00	2.58	1.89	2.51	1.65
16	1.70	1.68	2.14	3.07	2.17	2.47	1.56	1.75	1.60	0.46	0.78	1.46	1.77	1.21	2.26	1.42
19	2.29	2.13	2.87	3.32	2.27	1.42	1.10	1.44	1.24	0.48	0.94	1.37	1.61	1.22	2.03	1.49
23	2.94	3.45	4.32	4.30	2.66	0.88	1.51	1.50	1.22	0.48	1.25	1.37	1.44	1.19	2.40	1.36
27	3.72	4.56	5.42	4.65	2.68	1.30	1.66	1.70	1.22	0.44	1.50	1.53	1.53	1.44	2.31	1.67
31	4.54	5.66	6.22	4.61	2.80	1.43	1.71	1.69	1.15	0.37	1.74	1.85	1.70	1.66	2.13	2.14
35	5.31	6.45	5.88	4.49	2.86	1.51	1.61	1.56	1.07	0.32	1.97	2.18	1.36	1.78	2.19	2.53
39	6.50	7.58	5.56	4.28	3.08	1.58	1.42	1.41	1.02	0.35	2.22	2.49	1.37	1.95	2.39	3.06
43	7.19	7.63	5.28	3.83	2.56	1.57	1.27	1.19	0.80	0.35	2.43	2.60	1.10	1.89	2.13	3.34
47	7.76	6.87	4.53	2.52	2.67	1.52	1.11	0.83	0.68	0.22	2.60	2.58	0.89	1.68	1.90	3.73
51	7.48	6.00	3.41	2.81		1.35	0.97	0.71	0.70		2.63	2.33	0.69	1.42	1.59	3.57
55	7.54	5.48	3.01	2.33		1.20	0.73	0.67	0.57		2.55	1.86	0.49	1.06	1.07	2.98
59	6.08	4.88	2.94	2.12		1.09	0.55	0.66	0.52		2.38	1.55	0.16	0.93	0.93	2.70
65	5.54	3.83	2.07	1.88		0.91	0.44	0.56			2.10	1.29		0.73	0.70	2.31
73	4.57	3.05	1.45	2.01		0.71	0.27	0.33			1.82	0.98		0.53	0.48	1.96
81	3.66	2.17	1.53			0.49	0.13	0.24			1.51	0.76		0.42	0.43	1.55
89	2.92	1.75				0.36	0.13	0.17				0.63		0.37	0.40	1.23
97	2.47	1.48				0.29	0.05	0.17				0.54		0.33		1.06
105	1.98	1.76				0.23						0.47		0.27		0.94
113	1.61	3.19				0.21						0.47		0.28		1.07
121	1.23					0.20						0.50		0.33		1.30

The symbol $\int$ stands for a discrete sum when ϵ is related to discrete levels, and for $\int d\epsilon$ when one is concerned with continuum states. The function $g(E_1,E_2)$ is given by

$$g(E_1,E_2)=\frac{\alpha}{\pi}\frac{1}{E_1-E_2}\left\{\left(1+\frac{E_2^2}{E_1^2}\right)\ln\frac{2E_1}{mc^2}\sin\frac{\theta}{2}-\frac{E_2}{E_1}\right\}$$
$$+\frac{t}{2}\{\phi_{\text{coll}}(E_1,E_1-E_2)+\phi_{\text{rad}}(E_1,E_1-E_2)\}. \quad (32)$$

Here we have replaced the simple $\ln(2E_1/mc^2)$ by $\ln(2E_1/mc^2)\sin(\theta/2)$ so that the calibration with the low-photon emission case is more accurate.

We have already given the expressions for $g(E_1,E_2)$.[31] The cross section at fixed E_i, E_f, and θ is then given by an integral equation. In fact, it can be solved by repeated subtractions.

The simplest way to handle the continuum states is to divide the spectrum into small bands $\Delta\epsilon$ and to consider them as discrete levels peaked at ϵ, with width $\Delta\epsilon$. Given a spectrum with E_i, θ, one must know all the cross sections with incident energies $E_f+\epsilon<E_i$ at the same scattering angle, in order to apply the preceding equation (32) (Fig. 6). In practice, it has been applied as follows:

We measured different spectra at the same scattering angle with variable incident energies (say $E_i=75$, 100, 150, 180, 205, and 230 MeV). We first calculated the corrections to the elastic cross sections, at the above incident energies. We could therefore evaluate the radiative tails due to these elastic peaks, and this for all the incident energies E_i. The first transition level cross section was then subtracted from the elastic radiative tail contribution, and again corrected, and so on for every spectrum. The radiative tail of the first level could then be calculated. The elastic, and the first inelastic tails were then subtracted from the second-level cross section and again corrected.

The process was repeated for every spectrum, the continuum being divided into bands which were considered as inelastic discrete levels.

We emphasize the fact that for a radiative tail (elastic, inelastic, or continuum) corresponding to an incident energy E_1, and an excitation energy ϵ, one needs the cross sections corresponding to energies $E_f'>E_f$ (or excitation energies $\epsilon'<\epsilon$), which have already been calculated in the above treatment. Besides, one needs also the cross sections at incident energies E_i', which do not generally coincide with any E_i, but which are situated between two measured values ($E_i<E_i'<E_{i+1}$). We obtain them by interpolation, considering the cross sections as a function of q^2 for each ϵ, θ being invariable for all these spectra. For this interpolation, we took the inelastic cross sections as zero for null incident energy.

The results of this subtraction analysis on Be^9 are given in Table I in terms of $d^2\sigma_0/d\Omega dE_f|(d\sigma/d\Omega)_{\text{Mott}}$.

PART II—DATA ANALYSIS ON Be^9

We have shown how to extract the nuclear cross section from the measured spectra, either for discrete levels or for the continuum. We now show that in first Born approximation, in certain ranges of ϵ and q^2, we can extract all the cross sections at any given E_i, E_f, and θ

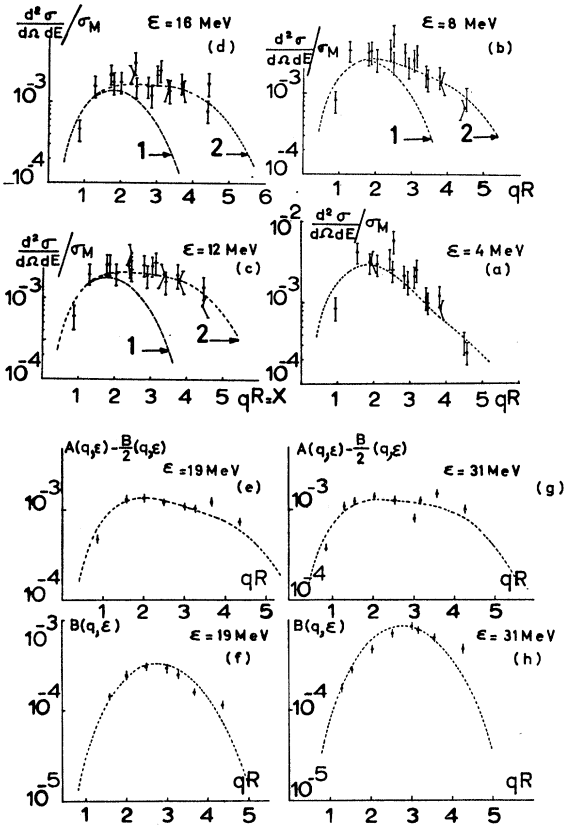

FIG. 7. Continuum inelastic form factors. For excitation energies $\epsilon<16$ MeV the cross section is dominated by the longitudinal term and we could express

$$\frac{d^2\sigma_0/d\Omega dE}{d\sigma/d\Omega_{\text{Mott}}}=[\lambda_1 j_1^2(qR)+\lambda_3 j_3^2(qR)]\exp(-q^2g^2).$$

For higher excitation energies it has been necessary to separate the angular dependence by

$$\frac{d^2\sigma/d\Omega dE}{d\sigma/d\Omega_{\text{Mott}}}=A(q^2,\epsilon)+B(q^2,\epsilon)tg^2\frac{\theta}{2}$$

and then analyze $A-B/2$ and B as function of q^2 for each determined.

(a) $\dfrac{d^2\sigma_0/d\Omega dE}{d\sigma/d\Omega_{\text{Mott}}}=[2.11j_1^2(x)+4.35j_3^2(x)]\times10^{-2}\exp(-0.095x^2)$;

(b) curve I $=1.86\times10^{-2}j_1^2(x)\exp(-0.095x^2)$; curve II $=[1.86j_1^2(x)+10.6j_3^2(x)]\times10^{-2}\exp(-0.095x^2)$;

(c) curve I $=1.34j_1^2(x)\times10^{-2}\exp(-0.095x^2)$; curve II $=[1.34j_1^2(x)+13.1j_3^2(x)]\times10^{-2}\exp(-0.095x^2)$;

(d) curve I $=1.04j_1^2(x)\times10^{-2}\exp(-0.095x^2)$; curve II $=[1.04j_1^2(x)+10.9j_3^2(x)]\times10^{-2}\exp(-0.095x^2)$;

(e) $[0.92j_1^2(x)+6.3j_3^2(x)]\times10^{-2}\exp(-0.095x^2)$;

(f) $0.85\times10^{-2}j_2^2(x)\exp(-0.095x^2)$;

(g) $[0.83j_1^2(x)+7.8j_3^2(x)]\times10^{-2}\exp(-0.095x^2)$;

(h) $2.16\times10^{-2}j_2^2(x)\exp(-0.095x^2)$.

$x=qR$.

in these same ranges from the nuclear cross sections just extracted.

The analysis is based on the general pattern of the one-photon-exchange cross section for the noncoincidence electron detection experiment.

$$\frac{d^2\sigma_0}{d\Omega dE_f}=\left(\frac{d\sigma}{d\Omega}\right)_{\text{Mott}}\left[A(q^2,\epsilon)+B(q^2,\epsilon)tg^2\frac{\theta}{2}\right], \quad (33)$$

where we use A and B as proportional respectively to F and G defined above.

In order to obtain A and B, we measured two series of spectra at fixed scattering angles of 60 and 135°. For every fixed pair of values q^2, ϵ, one can deduce the A and B.

In fact, we need some spectra at intermediate angles because the q^2 ranges, for 60 and 135°, are slightly different, and for each ϵ there is a range of nonoverlap for large q^2. In order to extend this overlap into the large q^2-value region, we used other spectra measured at 75 and 90°, whose radiative tails can be evaluated using the A and B form factors extracted from the spectra at 60 and 135°.

We have now obtained the experimental values of $A(q^2,\epsilon)$ and $B(q^2,\epsilon)$ for a large range of q^2 and ϵ.

We are now going to try to fit these functions with analytic forms. To do this, we notice that in analogy with the analysis for discrete elastic or inelastic levels, B would be related to transverse matrix elements and $A-B/2$ to longitudinal ones. We have then tried to fit the $A-B/2$ and B with the functional forms[32]

$$\sum_l \lambda_l(\epsilon)j_l^2(qR)e^{-q^2g^2}$$

for each determined ϵ, where R and g are parameters related to the extension of the density of transition.

The parameters R and g are assumed to be the same as for elastic and discrete inelastic transitions,[33] we wrote *a priori*

$$A-B/2=\sum_{l=1}^{4}\lambda_l(\epsilon)j_l^2(qR)e^{-q^2g^2} \quad (34)$$

and determined the $\lambda_l(\epsilon)$ by the least-square method in the case of a fixed ϵ. We limited ourselves to $l=4$, since $qR<5$ for all our experimental data. Hence, the contribution of higher components of the Bessel functions are completely negligible.

TABLE II. Example of the way in which the λ_l coefficients are chosen in the form factor analysis. The statistically non-null coefficients are λ_1 and λ_3.

$$A-\frac{B}{2}=\sum_{l=1}^{4}\lambda_l j_l^2(qR)\exp(-q^2g^2)$$

$\lambda_l\pm\Delta\lambda_l$	$\epsilon=19$ MeV	$\epsilon=39$ MeV
$l=1$	$(9.8\pm0.8)\times10^{-3}$	$(8.5\pm0.8)\times10^{-3}$
$l=2$	$(-1.2\pm0.8)\times10^{-2}$	$(-2.1\pm1.0)\times10^{-2}$
$l=3$	$(1.34\pm0.41)\times10^{-1}$	$(1.85\pm0.6)\times10^{-1}$
$l=4$	-0.167 ± 0.09	-0.23 ± 0.16

[31] H. Nguyen-Ngoc and J. Perez-y-Jorba, Compt. Rend. **255**, 3158 (1962).

[32] R. H. Helm, thesis, Stanford University 1956 (unpublished).

[33] H. Nguyen-Ngoc, M. Hors, and J. Perez-y-Jorba, Nucl. Phys. **42**, 62 (1963).

TABLE III. Results of the λ_l analysis.

ϵ MeV	λ_1	λ_2	λ_3	
4	$(2.11\pm0.22)\times10^{-2}$	0	0.043 ± 0.006	$\frac{d^2\sigma}{d\Omega dE}=\left(A+B\tg^2\frac{\theta}{2}\right)\frac{d\sigma}{d\Omega}$ Mott
8	$(1.86\pm0.22)\times10^{-2}$	0	0.106 ± 0.014	
12	$(1.34\pm0.17)\times10^{-2}$	0	0.131 ± 0.015	
16	$(1.04\pm0.14)\times10^{-2}$	0	0.109 ± 0.013	
19	$(0.925\pm0.09)\times10^{-2}$	$(0.85\pm0.06)\times10^{-2}$	0.063 ± 0.008	
23	$(0.856\pm0.09)\times10^{-2}$	$(1.48\pm0.11)\times10^{-2}$	0.065 ± 0.009	$A-\frac{B}{2}=(\lambda_1 j_1^2(x)+\lambda_3 j_3^2(x))e^{-q^2g^2}$
27	$(0.87\pm0.09)\times10^{-2}$	$(1.81\pm0.13)\times10^{-2}$	0.077 ± 0.010	
31	$(0.83\pm0.09)\times10^{-2}$	$(2.61\pm0.16)\times10^{-2}$	0.078 ± 0.010	
35	$(0.75\pm0.08)\times10^{-2}$	$(2.26\pm0.16)\times10^{-2}$	0.093 ± 0.012	$B=\lambda_2 j_2^2(x)e^{-q^2g^2}$
39	$(0.69\pm0.08)\times10^{-2}$	$(2.56\pm0.19)\times10^{-2}$	0.081 ± 0.010	
43	$(0.82\pm0.10)\times10^{-2}$	$(2.43\pm0.20)\times10^{-2}$	0.071 ± 0.010	$x=qR \quad R=2.75$ F
47	$(0.72\pm0.10)\times10^{-2}$	$(1.73\pm0.16)\times10^{-2}$	0.089 ± 0.014	$g=0.85$ F

In the Table II, we give some examples of results for this analysis in λ_1, λ_2, λ_3, and λ_4 on the Be^9 data.

For all $\epsilon<47$ MeV, we found the somewhat unexpected result that λ_2 and λ_4 are null within statistics. We then tried to fit $(A-B/2)$ with the form

$$A-B/2=[\lambda_1(\epsilon)j_1^2(qR)+\lambda_3(\epsilon)j_3^2(qR)]e^{-q^2g^2} \quad (35)$$

and determined $\lambda_1(\epsilon)$ and $\lambda_3(\epsilon)$ with their errors.

The same analysis in λ_1, λ_2, λ_3, and λ_4 was used for B. But it became apparent after trials that one can obtain a good fit with only one coefficient λ_2 and B would then be in the form

$$B=\lambda_2(\epsilon)j_2^2(qR)e^{-q^2g^2}. \quad (36)$$

Figure 7 shows the fit of $A-B/2$ and B with the adopted analytical forms for some ϵ.

The final results on λ_l analysis are recorded in Table III.

We must emphasize that the A and B given in this analysis, even at low-excitation energy ($\epsilon<10$ MeV) concern the continuum. The form factors of the discrete excited levels have been studied elsewhere[33] and subtraction of these known excited state nuclear cross sections has been applied here.

We now reach one of the aims of this analysis, which is to get the cross section at any E_i, θ, ϵ (or equivalently q^2), provided that q^2 and ϵ are within the range of our available form factors. Indeed, from Eq. (33) it is obvious that for any couple q^2, ϵ, one has only to determine from Table III, the corresponding A and B, and thence calculate the nuclear cross section. This is extremely interesting, since one can determine, by this technique, the cross section for very high energy and small scattering angle (and hence small q^2) by measuring the cross section at lower energy, backward angle, and the same q^2 value.

A. Verification of the Validity of the Method

In order to verify the validity of the subtraction method used, two kinds of tests have been carried out: Firstly, a "weak" test which aims to control the internal consistency of the formulation, and secondly, a "strong" test which verifies the possibility of extracting new nuclear cross sections.

1. Consistency of the Analysis

Let us consider a measured spectrum s, and let s_1 be the subtracted spectrum in the manner already described. Now let us proceed to the subtraction of s by using the "expected to be true" form factors already obtained. A second spectrum s_2 is then evaluated. If the analysis is self-consistent, then s_1 and s_2 should coincide. For the sake of convenience, the ratio s_1/s_2 has been shown instead of s_1 and s_2 separately, as

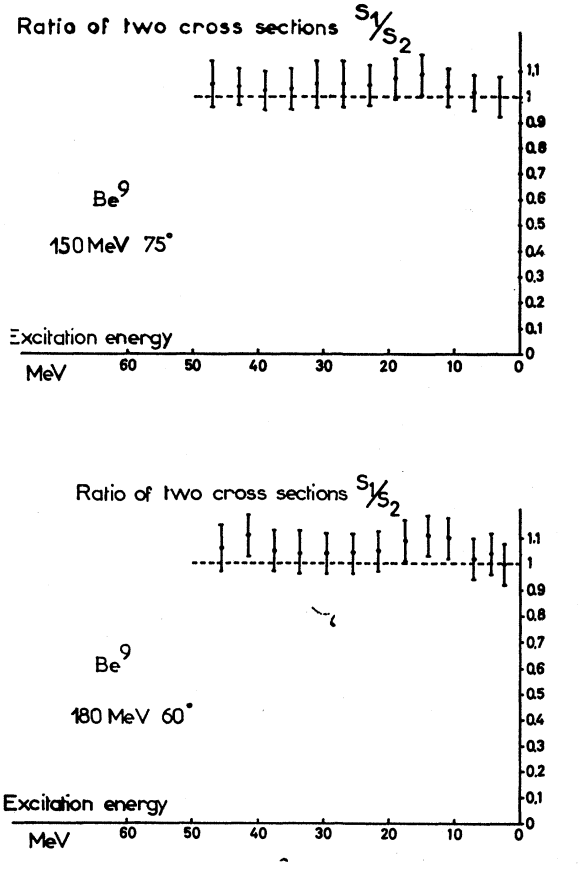

FIG. 8. Test on the analysis consistency. The ordinate represents the ratio of two spectra obtained from the same experimental spectrum by two different subtractions.

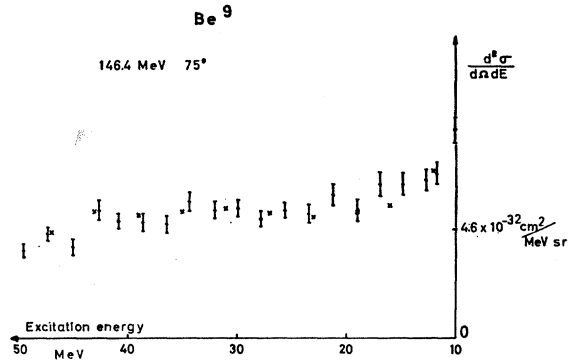

FIG. 9. Test on the possibility of extracting new cross sections. The crosses represent the cross sections calculated from Table III obtained from a limited number of experimental spectra. The points with errors bars represent the measured experimental spectrum (these points are not related to the set of data allowing the calculation of Table III).

a function of the excitation energy. Two spectra have been tested in this way and Fig. 8 demonstrates convincingly the consistency of the analysis.

2. *Extraction of New Data*

Beginning with the determined form factors $A(q^2,\epsilon)$ and $B(q^2,\epsilon)$ we constructed, in reverse, one spectrum with given incident energy E_i, and scattering angle θ. This spectrum has no connection with the ones used for the extraction of the A and B. We first determined the elastic form factor and evaluated the elastic radiative tail. The process was repeated for other inelastic levels, and all the cross sections at the same final energy (or equivalently at same excitation energy ϵ) were summed up. The continuum spectrum was divided, as before, into small bands of 4-MeV width.

We thus obtain a complete spectrum exactly similar in form with the result of an experiment, except that it was not measured experimentally, but determined as the result of the above analysis.

Next, we measured, experimentally, the spectrum corresponding to the same conditions (E_i,θ), and compared it to the one above.

Figure 9 shows the excellent fit obtained. Essentially, this second test proves two things: (1) The effects of the approximation done on the calculation of the radiative tail are not important as long as the value of ϵ is not too large. (2) The analysis is general and allows the concentration from a limited number of measured spectra of any spectrum at any given incident energy and scattering angle, provided that the square four momentum and the excitation energy are in the range of the measured ones.

It is encouraging to observe that with a high-speed electronic computer, the radiative tail could be calculated with more precision by numerical integration.

As we were limited by the partial overlapping of the q^2 value, and as q^2 and ϵ are related for fixed E and θ, we could not make a complete A and B analysis of the data for $\epsilon > 47$ MeV.

Finally, we would emphasize that the choice of the width $\Delta\epsilon$ (4 MeV in this analysis), introduced in the continuum subtraction, is not critical. For one spectrum we have used twice that width, and the two results are practically identical.

B. Discussion of Errors

There are, in general, two categories of errors, those which affect directly the experimental measurements and those which are introduced by the analysis procedure applied to the data. The first type of error is due to uncertainties in the evaluation of experimental parameters, such as target thicknesses, scattering angle, solid angle and dispersion of the spectrometer, calibrations of the energy, the current monitor, and finally, counting statistics. These errors can be evaluated accurately, and in our conditions they vary from 5 to 7% per band of energy used. The second type of error, which is due mainly to the subtraction of the radiative tail, as well as to the way we extract our invariants, cannot be estimated so well. In principle, the statistical errors can be calculated as the subtractions involved are linear processes. Hence, error analysis techniques would permit their accurate calculation. However, in our cases, too many approximations have been used and such an elaborate analysis is almost useless.

Nevertheless, the test we applied to our analyzed data allows us to estimate the total error as being around 12%, but less than 15% in any case.

C. Attempts at Interpretation

As far as we know, at the present time there is no reliable theory of the continuous spectrum in inelastic electron scattering on light nuclei. Some approximate attempts at a theoretical interpretation have been made, such as bringing into use the harmonic oscillator wave function,[34,4] in order to calculate the charge interaction matrix element in the independent-particle shell model. Another method is to interpret the inelastic "bump" as being due to scattering on quasiparticles. This means that the process is purely incoherent, and the cross section is simply the sum of individual cross sections with quasifree nucleons.[7]

Recently, Czyz[5] introduced the second quantization and expressed the cross sections in terms of the response functions. However, for practical application, he had recourse to a Fermi gas model, requiring a nuclear matter with equal number of protons and neutrons.

These model-dependent calculations rely on assumptions which are more or less valid in the case of a real nucleus like Be^9. The subsequent fit is then limited by the various approximations assumed in the models.

[34] E. Amaldi, G. Fidecaro, and F. Mariani, Nuovo Cimento 7, 553 (1950).

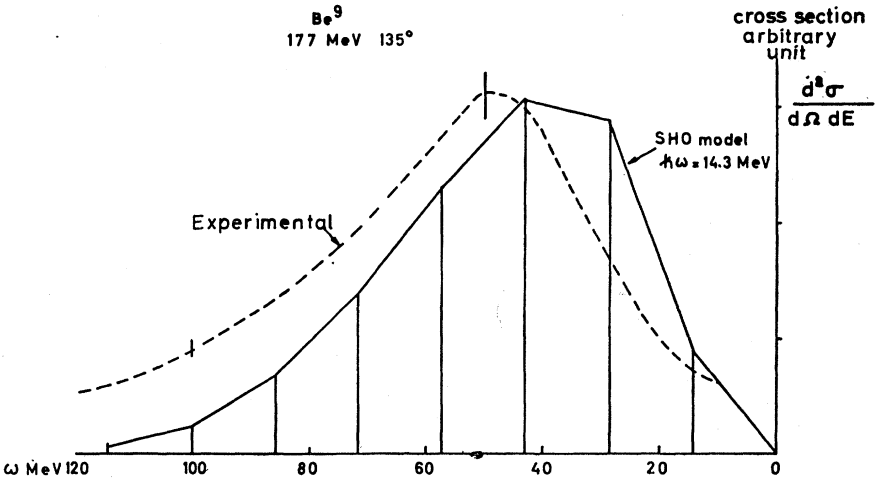

FIG. 10. Comparison of the measured cross section with calculations on the basis of the harmonic oscillator model. The theoretical lines have been multiplied by a factor 4 to obtain the same maximum. The calculated cross section is too low.

The harmonic oscillator deals with discrete transitions with equal energy spacings, which is far from being the case here. The incoherent impulse approximation requires a momentum transfer much larger than for the cases we considered here.

And, finally, our nucleus is too light to be considered as a Fermi gas, as in the third model studied below.

1. Harmonic Oscillator Model

This has been considered by Amaldi *et al.*,[34] who gave, in particular, the angular variation of spectrum forms for 600-MeV incident muons scattered by C^{12} and Li^7. Calculations along the same line have also been given by Bishop[4] who considered only the charge interaction, for which the result can be written as follows:

$$d\sigma/d\Omega=\sigma_{\text{proton}}\sum\beta_{mn}|\chi_{mn}|^2, \tag{37}$$

where β_{mn} comes from kinematical factor

$$\beta_{mn}=\left[1+\frac{\delta^2}{4(1-\delta)\sin^2(\theta/2)}\right]^{-2},$$

and δ relates the energy of transition between the states m and n, and the incident energy E_i

$$\delta E_i=(m-n)\hbar\omega,$$

$\hbar\omega$ being the quantum of the oscillator.

χ_{mn} is defined by

$$\chi_{mn}=\rho_{mn}(x)\exp(-x),$$

with $x=q^2a^2/2$; $a=(\hbar^2/M_{\text{proton}}\omega)^{1/2}$ is the oscillator parameter

$$\rho_{0m}(x)=x^m/m!\quad \rho_{1m}(x)=x^{m-1}(x-m)^2/m!.$$

For Be^9, it turns out that

$$\sum\beta_{mn}|\chi_{mn}|^2=\frac{10}{3}\sum_{m=1}^{\infty}\beta_{0m}|\chi_{0m}|^2-\tfrac{2}{3}\beta_{01}|\chi_{01}|^2+\tfrac{2}{3}\sum_{m=2}^{\infty}\beta_{1m}|\chi_{1m}|^2. \tag{38}$$

The cross section σ_{proton} is the charge cross section, but it has been assumed to be the experimental electron proton cross section in order to account, in a rough way, for the magnetic interaction with the electron.

It is clear that one can only compare the sum of the calculated lines with the area under the continuous spectrum (Fig. 10). We obtain for a spectrum at 177-MeV 135°:

Oscillator	$\int_{}^{90\text{ MeV}}(d^2\sigma/d\Omega dE)dE_{\text{experimental}}$	$Z\sigma_p+N\sigma_N$
5.7×10^{-32} cm²/sr	$(22\pm2)\times10^{-32}$ cm²/sr	31×10^{-32} cm²/sr.

Thus, there is a distinct discrepancy when compared with the oscillator model. The third value calculated above ($Z\sigma_p+N\sigma_N$) is the sum of incoherent cross sections on individual free nucleons. It would seem that the incoherent scattering is more acceptable.

2. Incoherent Scattering

In fact, many authors have succeeded in explaining the quasielastic bump, due to electron scattering on C^{12}, by purely incoherent process.[6,7] We refer here to the

calculations given by Potter[7] who considered that the initial nucleon possessed a momentum in the laboratory frame. The over-all cross section is then assumed to be the sum of electron scattering on individual nucleons. The result is

$$\frac{d^2\sigma}{d\Omega dE}=e^4\frac{k'}{k}\frac{(I_1+I_2)}{q^4},$$

where

$$I_1=\frac{2\pi}{|\mathbf{q}|}\frac{q^2}{4}\Big[-4M^2F_1^2+q^2\Big(1-\frac{q^2}{2M^2}\Big)K^2F_2^2+4q^2KF_1F_2\Big]J_3, \quad (39)$$

$$I_2=\frac{2\pi}{|\mathbf{q}|}\Big[F_1^2+\frac{q^2}{4M^2}K^2F_2^2\Big][T_1J_1+T_2J_2+T_3J_3].$$

We have simplified without approximation the expressions given for T_1 and T_2 in Ref. 7.

$$T_1=(q^4/|\mathbf{q}|^4)[(k+k')^2+2kk'\cos^2(\theta/2)],$$

$$T_2=q_0T_1,$$

$$T_3=-\Big(M^2\mathbf{q}^2+\frac{q^4}{4}\Big)\frac{k^2+k'^2}{\mathbf{q}^2}+(M^2\mathbf{q}^2+\tfrac{3}{4}q^4)[(\mathbf{k}\cdot\mathbf{q})^2+(\mathbf{k}'\cdot\mathbf{q})^2]\frac{1}{\mathbf{q}^4},$$

and (40)

$$J_1=\int_{p_{\min}}^{p_{\max}}p(p^2+M^2)^{1/2}N(p)dp,$$

$$J_2=\int_{p_{\min}}^{p_{\max}}pN(p)dp,$$

$$J_3=\int_{p_{\min}}^{p_{\max}}\frac{p}{(p^2+M^2)^{1/2}}N(p)dp.$$

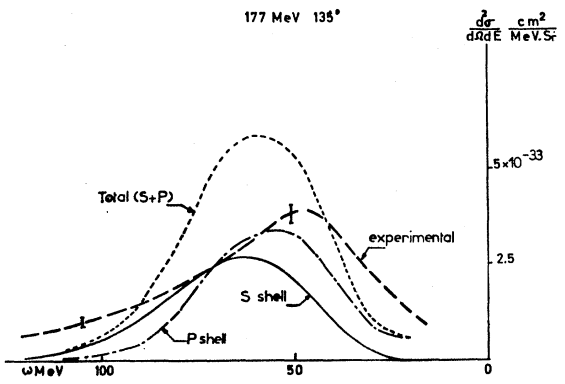

FIG. 11. Comparison of the measured cross section with the cross section calculated on the assumption of incoherent processes, in which a nucleon is ejected. Separate contributions of the s shell and p shell are shown, as well as the total contribution.

Here the various quantities are defined as follows:

$$\begin{aligned}&\mathbf{q}=\mathbf{k}-\mathbf{k}' \quad \text{3-momentum transfer to the nucleon;}\\ &q^2=\mathbf{q}^2-q_0^2 \quad \text{4-momentum transfer to the nucleon;}\\ &|\mathbf{k}|=k \quad \text{incident electron energy;}\\ &|\mathbf{k}'|=k' \quad \text{scattered electron energy;}\\ &p_{\max}=|\mathbf{q}|+[(2M+q_0-B)(q_0-B)]^{1/2},\\ &p_{\min}=|\mathbf{q}|-[(2M+q_0-B)(q_0-B)]^{1/2}.\end{aligned} \quad (41)$$

$N(p)$ represents the momentum distribution of the nucleon inside the nucleus, and B its binding energy. In calculating $N(p)$ from the harmonic oscillator wave functions, one can evaluate the integrals J_1, J_2, and J_3 very simply by assuming that $p\ll M$ the nucleon mass.

We obtained the proton oscillator parameters from the $(p,2p)$ experiment.[35]

$$N_s(p)=(1/\pi^{3/2}p_a^3)e^{-p^2/p_a^2},$$
$$N_p(p)=(2/3\pi^{3/2}p_a^3)(p^2/p_a^2)e^{-p^2/p_a^2}. \quad (42)$$

	s shell	p shell
proton	$B=26$ MeV	$B=17.2$ MeV
	$p_a=105$ MeV	$p_a=65$ MeV
neutron	$B=26$ MeV	$B=1.66$ MeV
	$p_a=150$ MeV	$p_a=120$ MeV.

The p-shell neutron binding energy is known[36] and we assumed the same binding energy for neutrons and protons of the s shell. However, we have increased the oscillator parameters p_a for s-shell and p-shell neutrons so that we obtain a better fit for the shape of the calculated curve. We find that the absolute value of the maximum is not strongly affected by the variation of p_a (Fig. 11).

The same kind of fit has also been obtained for[37] Al^{27} in the same range of energy. One can reasonably deduce that the nucleon ejection is only a part of the quasi-elastic processes, at least for these momentum transfer ranges.

3. *Impulse Approximation Using the Fermi Gas Model*

Considering the nucleus as an assembly of nucleons, Czyz[5] used the electron nucleon Hamiltonian, given by Mc Voy *et al.*,[38] valid to the order q^2/M^2 and expressed the cross section in terms of the response functions, by means of second quantization techniques. Using the Fermi gas model to evaluate these response functions, the result can be given in a simple form

$$\frac{d^2\sigma}{d\Omega dE}=\Big(\frac{d\sigma}{d\Omega}\Big)_{\text{Mott}}^{\text{proton}}f^2(q^2)\frac{2}{(p_a\sqrt{\pi})^3}\times[\text{“}QQ\text{”}+\text{“}JQ\text{”}+\text{“}JJ\text{”}], \quad (43)$$

[35] J. P. Garron, thesis, Université de Paris, 1962 (unpublished).
[36] F. Ajzenberg Selove and T. Lauritsen, Nucl. Phys. **11**, 1 (1959).
[37] J. Chollet, Internal Report, 1091, Linear Accelerator Laboratory, Orsay, 1963 (unpublished).
[38] K. W. McVoy and L. Van Hove, Phys. Rev. **125**, 1034 (1962).

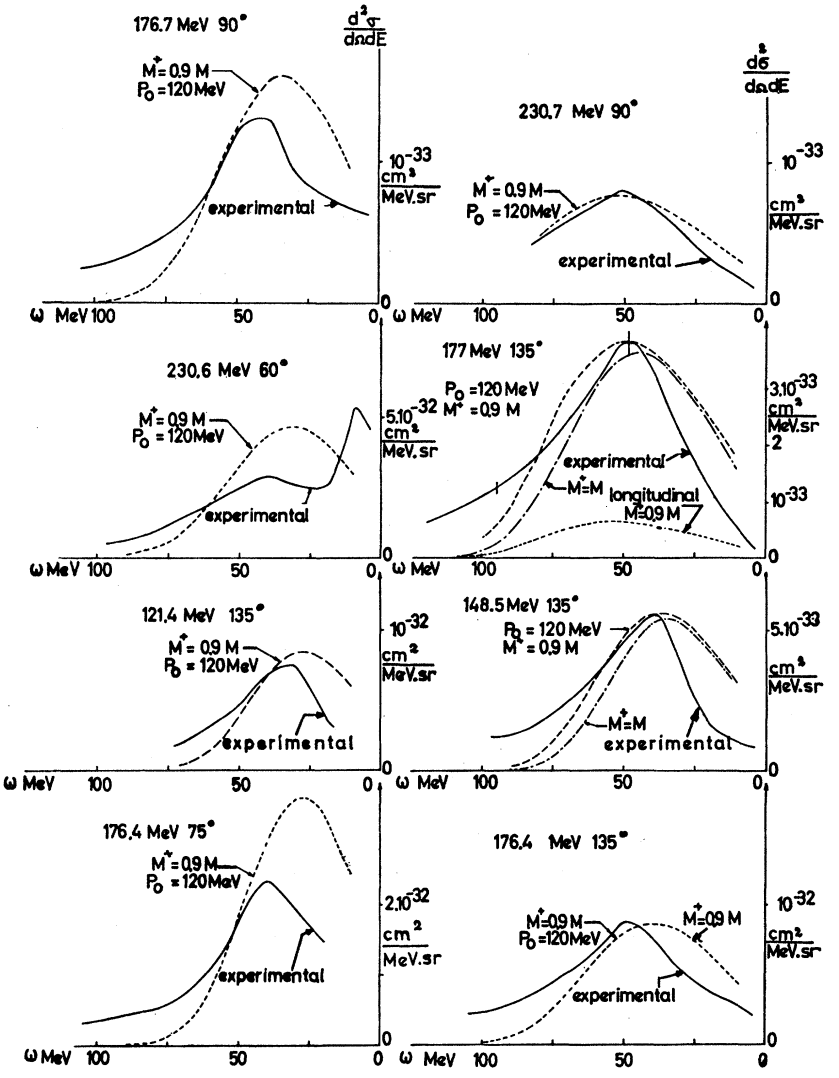

FIG. 12. Comparison with the calculated cross section of a Fermi gas model. M^* represents the effective mass of the nucleon.

where we use the following approximation (1) for nucleon form factors

$$F_1^{(p)}=F_2^{(p)}=F_2^{(n)}=f(q^2)=(1+q^2a_1^2)^{-2},$$

with $a_1\sqrt{12}=0.8$ F, $F_1^{(n)}=0$.

The three terms in the bracket are related, respectively, to the density-density correlation, the density current and the current-current correlation.

$$\begin{aligned}
&\text{“}QQ\text{”}=\frac{2}{\pi}\left[1-\frac{q^2}{4M^2}(1+2K)\right]I,\\
&\text{“}QJ\text{”}=\frac{-2}{\pi}\frac{\omega}{Mq}[2Q_1+q]I,\\
&\text{“}JJ\text{”}=\frac{2}{\pi}\frac{\omega^2}{q^2M^2}\left[q\Omega_1+\tfrac{3}{2}\Omega_2-\frac{G}{2}-\frac{K(K+1)}{2}\times q^2\right]I\\
&\qquad+\frac{2}{\pi}\frac{1}{M^2}\left(\frac{1}{2}+tg^2\frac{\theta}{2}\right)[G-\Omega_2+q^2(\tfrac{1}{2}+K+K^2)]I.
\end{aligned}\tag{44}$$

In these formulas, K represents the anomalous magnetic moment of the nucleon of mass M; ω is the energy transfer. If the momentum distribution of the nucleon is that of a Fermi gas, Ω_1 and Ω_2 are reduced to

$$\Omega_2=\Omega_1^2;$$
$$\Omega_1=M\omega/q-q/2.$$

Besides

$$\begin{aligned}
&I=\int n(|\mathbf{k}|)[1-n(|\mathbf{k}+\mathbf{q}|)]\mathbf{dk}\delta[\omega-E(k+q)+E(k)],\\
&G=I^{-1}\int n(|\mathbf{k}|)[1-n(|\mathbf{k}+\mathbf{q}|)]k^2d\mathbf{k}\\
&\qquad\times\delta[\omega-E(k+q)+E(k)].
\end{aligned}\tag{45}$$

Normally, $n(|\mathbf{k}|)$ is the Fermi momentum distribution (step function). Czyz suggested, however, using the shell-model distribution. For $1p$ shell we can write

$$n(p)=[1+\alpha(p^2/p_a^2)]\exp(-p^2/p_a^2),\tag{46}$$

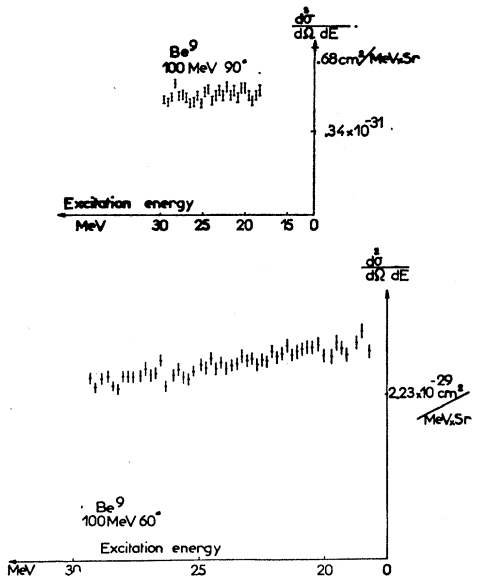

FIG. 13. Electron scattering on Be^9 around the giant resonance excitation.

with $\alpha=(A-4)/6$, where A is the mass number of the nucleus and $p_a=\hbar/a$ the oscillator parameter. The integrals I and G can easily be evaluated to give

$$I=\frac{\pi M}{q}p_a^2\Big[M_{10}+\alpha M_{11}-(\beta M_{20}+\alpha(1+\beta)M_{21}+\alpha^2 M_{22})\exp\frac{1-\beta}{\alpha}\Big],$$

$$G=\frac{\pi M}{qI}p_a^4\Big[M_{12}+\alpha M_{13}-(\beta M_{22}+\alpha(1+\beta)M_{23}+\alpha^2 M_{24})\exp\frac{1-\beta}{\alpha}\Big],$$

where

$$\beta=1+(2M\omega/p_a^2)\alpha,$$

$$M_{mn}=\int_{x_0}^{\infty}e^{-mx}x^m dx,$$

$$x_0=\Omega_1^2/p_a.$$

The expressions of M_{mn} can be obtained from the lowest moment by successive derivation with respect to m.

The results are shown on Fig. 12, where we notice a poor fit for low transfers. However, for high-momentum transfers the correct order of magnitude is obtained, particularly as there was only one adjustable parameter.

Of the three considered models, the last one seems to give the best fit, as much for the form of the spectra, as for the order of magnitude of the cross sections. Unfortunately, it is not possible to draw any definite conclusion since, as we have said, the nucleus in question is too light to be considered as a gas of nucleons, and the cluster structure found in the discrete level analysis[33] would conflict with the simple momentum energy relation for a Fermi gas particle.

D. Giant Resonance

One of the aims of this study was to try to observe the giant resonance structure of the Be^9 nucleus. In our experiments (Fig. 13) we did not see any resonance similar to the one observed in the reactions[39,40]

$$Be^9(\gamma n)Be^8 \quad \text{or} \quad Be^9(\gamma p)Li^8.$$

Measurements on gamma-ray scattering with a betatron[41] had also failed to observe this resonance. On the other hand, Goldemberg[42] measured spectra of 180° electron scattering on Be^9 at 40- and 70-MeV incident energies, and did not see the giant resonance which he observed on other nuclei.

We would point out that if the giant resonance excitation cross section is calculated approximately, by electron scattering, using the known photoreaction cross section, a cross section, easily detectable by electron scattering, would be found.

From the three independent negative results, one can state that the open channels are certainly numerous, and hence the giant resonance is completely masked in these experiments.

CONCLUSION

The results of this study have been twofold. Firstly, we have given a general method, in first Born approximation, of extracting electrodisintegration cross sections in given ranges of ϵ and q^2 values, and for any incident energy and scattering angle corresponding to these ranges. In this study, we have been led to give a general formula for the radiative scattering processes. The connection with the formulas proposed by other authors has been shown. Checks have been made of the validity of various stages of the process.

Secondly, these techniques have been applied to the study of the continuum of a light element Be^9, and the corresponding cross sections have been obtained. Then, different approximate models have been compared with the results, but the degree of conformity can be considered as satisfactory only for the Fermi gas model.

The form of the spectrum at high excitation energy is strongly related to the correlation between the nucleons. Hence, any progress in the interpretation of the continuum cross sections would contribute to the understanding of the nuclear structure. A parallel effort must be made to obtain the experimental data on other nuclei.

---

[39] R. Nathans and J. Halpern, Phys. Rev. **92**, 940 (1953).
[40] R. N. H. Haslam, L. Katz, E. H. Crosby, R. G. Summers-Gill, and A. G. W. Cameron, Can. J. Phys. **31**, 210 (1953).
[41] M. Langevin and M. Loiseau (private communication).
[42] J. Goldemberg (private communication).

We may emphasize the fact that, from these measurements at low energies, it is possible to calculate the form factors for high-energy processes at forward angles, which would be hard to measure directly. This could be helpful, for example, in calculating lepton pair production by a neutrino beam.[43]

ACKNOWLEDGMENTS

We are grateful to Professor Blanc-Lapierre for extending to us the hospitality of the Orsay Linear Accelator Laboratory and to Professor Bishop, with whom we have had helpful discussions. We are indebted to Dr. Aggson, Dr. Frerejacque, Dr. Isabelle, and Dr. Parikh for their assistance in taking the data. Finally, it is with pleasure that we thank the team of engineers directed by Dr. Burnod, Dr. Milman, and Dr. Round for giving us many trouble-free nights and for helping with the experimental setup.

Here we should also like to thank Dr. Langevin and Dr. Loiseau of the Frederic Joliot Laboratory, Orsay, and Dr. J. Goldemberg and Dr. W. Czyz of Stanford University for making known to us their results, before publication.

APPENDIX

In the frame of reference where $\mathbf{p}_A=0$, one may choose the axis as follows

$$\hat{z}=\frac{\mathbf{s}-\mathbf{p}}{|\mathbf{s}-\mathbf{p}|}, \quad \hat{y}=\frac{\mathbf{s}\times\mathbf{p}}{|\mathbf{s}\times\mathbf{p}|}, \quad \hat{x}=\hat{y}\times\hat{z}.$$

Defining $u=s-p+p_A$ one finds easily from $p_B=u-k$

$$\omega=\frac{u^2-M_B{}^2}{2[u_0-|\mathbf{u}|\cos\theta_k]}, \tag{A1}$$

with

$$\theta_k=(\mathbf{u},\mathbf{k})$$

$$\varphi_k=(\text{planes } \mathbf{uk};\ \mathbf{s},\ \mathbf{p}).$$

Hence

$$k\cdot s=\omega[E_s-s_z\cos\theta_k-s_x\sin\theta_k\cos\varphi_k],$$
$$k\cdot p=\omega[E_p-p_z\cos\theta_k-p_x\sin\theta_k\cos\varphi_k], \tag{A2}$$

where

$$s_x=p_x=\frac{|\mathbf{s}\times\mathbf{p}|}{|\mathbf{u}|}=\frac{\mathbf{s}^2\mathbf{p}^2-(\mathbf{s}\cdot\mathbf{p})^2}{|\mathbf{s}-\mathbf{p}||\mathbf{s}\times\mathbf{p}|},$$

$$s_z=\mathbf{s}\cdot(\mathbf{s}-\mathbf{p})/|\mathbf{s}-\mathbf{p}|,$$

$$p_z=\mathbf{p}\cdot(\mathbf{s}-\mathbf{p})/|\mathbf{s}-\mathbf{p}|.$$

It follows that

$$\int_0^{2\pi}\frac{d\varphi_k}{k\cdot s}=\frac{2\pi}{\omega|\mathbf{s}|\lambda_s{}^{1/2}}; \quad \int_0^{2\pi}\frac{d\varphi_k}{k\cdot p}=\frac{2\pi}{\omega|\mathbf{p}|\lambda_p{}^{1/2}},$$

$$\int_0^{2\pi}\frac{d\varphi_k}{(k\cdot s)^2}=\frac{2\pi}{\omega^2|\mathbf{s}|E_s}\left[\frac{E_s{}^2}{m^2}\eta_s{}^2-X_s(X-X_s)\right]\frac{1}{\lambda_s{}^{3/2}}, \tag{A3}$$

$$\int_0^{2\pi}\frac{d\varphi_k}{(k\cdot p)^2}=\frac{2\pi}{\omega^2|\mathbf{p}|E_p}\left[\frac{E_p{}^2}{m^2}\eta_p{}^2-X_p(X-X_p)\right]\frac{1}{\lambda_p{}^{3/2}},$$

with the following definitions:

$$\begin{aligned}&\lambda_j=(X-X_j)^2+\eta_j{}^2,\\ &X=\cos\theta_k,\\ &X_s=E_s s_z/\mathbf{s}^2, \quad X_p=E_p p_z/\mathbf{p}^2,\\ &\eta_s=m(s_x/\mathbf{s}^2), \quad \eta_p=m(p_x/\mathbf{p}^2).\end{aligned} \tag{A4}$$

Since

$$q^2=(s-p-k)^2=(s-p)^2-2\omega(E_s-E_p)+2\omega|\mathbf{u}|X.$$

One can integrate $S_{\mu\nu}T_{\mu\nu}$ over $d\varphi_k$ using the above integrals.

Noting that λ_s and λ_p become extremely small when X approaches X_s or X_p, we have arranged the numerator terms in the form $X-X_s$ or $X-X_p$ and this gives a good idea of relative importance of different terms.

One is left with an integral over

$$\int_{-1}^{+1}dX$$

which can be transformed to

$$\int_{q\min}^{q\max}dq^2$$

since q^2 and X are linearly dependent.

The cross sections are given by formulas (15) or (16) in the text. The result of integration over $d\varphi_k$ can be

[43] W. Czyz and J. D. Walecka, Phys. Letters 8, 77 (1964).

written as follows:

$$\int_0^{2\pi} S_{\mu\nu}T_{\mu\nu}d\varphi_k=\frac{\pi M_A{}^2}{m^2}F(q^2)\Big\{\Big[2E_p(E_s-\omega)+\frac{q^2}{2}\Big]\Big[-(X-X_s)^2+\frac{m^2X_s}{\omega E_s}(X-X_s)-\eta_s{}^2\frac{E_s+\omega}{\omega}\Big]\frac{1}{\omega|\mathbf{s}|\lambda_s{}^{3/2}}$$

$$+\Big[2E_s(E_p+\omega)+\frac{q^2}{2}\Big]\Big[(X-X_p)^2+\frac{m^2X_p}{\omega E_p}(X-X_p)-\eta_p{}^2\frac{E_p-\omega}{\omega}\Big]\frac{1}{\omega|\mathbf{p}|\lambda_p{}^{3/2}}$$

$$-2+\frac{2}{\omega^2}\Big[\frac{1}{|\mathbf{p}|\lambda_p{}^{1/2}}-\frac{1}{|\mathbf{s}|\lambda_s{}^{1/2}}\Big]\big[m^2(s\cdot p-\omega^2)+s\cdot p(E_sE_p+\mathbf{s}\cdot\mathbf{p}+\omega(E_s-E_p))\big]\frac{1}{E_s-E_p-|\mathbf{u}|X}$$

$$+(m^2+s\cdot p-2E_s{}^2)\frac{1}{\omega|\mathbf{s}|\lambda_s{}^{1/2}}-(m^2+s\cdot p-2E_p{}^2)\frac{1}{\omega|\mathbf{p}|\lambda_p{}^{1/2}}\Big\}$$

$$+\frac{\pi G(q^2)}{m^2}\Big\{-m^2(q^2+2m^2)\Big[\frac{E_s{}^2\eta_s{}^2m^{-2}-X_s(X-X_s)}{\omega^2|\mathbf{s}|E_s\lambda_s{}^{3/2}}+\frac{E_p{}^2\eta_p{}^2m^{-2}-X_p(X-X_p)}{\omega^2|\mathbf{p}|E_p\lambda_p{}^{3/2}}\Big]$$

$$-4+(q^2-2m^2+6s\cdot p)\Big[\frac{1}{|\mathbf{p}|\lambda_p{}^{1/2}}-\frac{1}{|\mathbf{s}|\lambda_s{}^{1/2}}\Big]\frac{1}{\omega}$$

$$+4s\cdot p(q^2+s\cdot p)\Big[\frac{1}{|\mathbf{p}|\lambda_p{}^{1/2}}-\frac{1}{|\mathbf{s}|\lambda_s{}^{1/2}}\Big]\frac{1}{\omega^2[E_s-E_p-|\mathbf{u}|X]}\Big\}, \quad \text{(A5)}$$

where $(s\cdot p=E_sE_p-\mathbf{s}\cdot\mathbf{p})$.